PNAS Nexus, 2024, 3, 1–8
https://doi.org/10.1093/pnasnexus/pgad443
Advance access publication 20 December 2023
Research Report

Computer simulations predict the impact of neuronal atrophy on the calcium dynamics in Huntington's disease

Sara Sameni [a,b], Thomas M. Bartol Jr[b], Jody Corey-Bloom[c] and Terrence J. Sejnowski [a,b,*]

[a]Division of Biological Sciences, University of California, San Diego, CA 92093, USA
[b]Computational Neurobiology Laboratory, Salk Institute, La Jolla, CA 92037, USA
[c]Department of Neurosciences, University of California San Diego, San Diego, CA 92093, USA
*To whom correspondence should be addressed: Email: ssameni@salk.edu
Edited By: Ivet Bahar

Abstract

One of the early hallmarks of Huntington's disease (HD) is neuronal cell atrophy, especially in the striatum, underlying motor dysfunction in HD. Here using a computer model, we have predicted the impact of cell shrinkage on calcium dynamics at the cellular level. Our model indicates that as cytosolic volume decreases, the amplitude of calcium transients increases and the endoplasmic reticulum (ER) becomes more leaky due to calcium-induced calcium release and a "toxic" positive feedback mechanism mediated by ryanodine receptors that greatly increases calcium release into the cytosol. The excessive calcium release from ER saturates the calcium buffering capacity of calbindin and forces further accumulation of free calcium in the cytosol and cellular compartments including mitochondria. This leads to imbalance of calcium in both cytosol and ER regions. Excessive calcium accumulation in the cytosol can damage the mitochondria resulting in metabolic dysfunction in the cell consistent with the pathology of HD. Our computational model points toward potential drug targets and can accelerate and greatly help the experimental studies of HD paving the way for treatments of patients suffering from HD.

Keywords: Huntington's disease, computational model, calcium metabolism, aging, biomarkers

Significance Statement

There are presently no effective treatments for Huntington's disease (HD). We present a computational model of neuronal cell atrophy during HD which predicts that cell shrinkage contributes to dysfunction of calcium dynamics and cell pathology. The model identifies calbindin, ryanodine receptors, and dihydropyridine receptors as potential drug targets to address the dysfunction. Neuronal cell atrophy is seen in aging and other neurodegenerative disorders, thus our in silico model could be used to develop new biomarkers and to predict the efficacy of treatments at an early stage of neurodegeneration.

Introduction

There is great interest in calcium metabolism and homeostasis in neurodegenerative disorders and aging. An earlier study showed how cellular metabolism is affected in Huntington's disease (HD) (1). During the course of HD, cells, especially in the striatal region and cortex, shrink, and eventually die (2–4). Brain atrophy in HD is correlated with the duration of the disease (5). In recent studies, the rate of disease progression has been accurately estimated by measuring atrophy rates in preclinical HD subjects compared to controls (3, 6).

HD is an autosomal dominant inherited neurological disorder caused by the expansion of cytosine–adenine–guanine (CAG) repeats in exon1 of the gene coding for the Huntingtin protein. One of the hallmarks of HD is the atrophy of multiple brain regions including the striatum and other subcortical gray matter and cortical brain areas in premanifest HD gene carriers. Huntingtin is widely expressed in neuronal cells; however, it is also widely expressed in non-neuronal peripheral tissue including the heart, skeletal muscle, liver, and kidneys. Loss of body mass and muscle atrophy are hallmarks of HD (7–9). It has also been shown that the same pathway that leads to neurodegeneration in HD is also active in myoblast and blood cell cultures taken from HD patients, contributing to mortality (10, 11). There is a regional brain atrophy reported in HD which progresses based on the disease severity. Late in the disease volumetric losses of the following magnitudes are observed: 20% in cortex, 30% in thalamus, 30% in cerebral white matter, 55% in globus pallidus, and 60% in striatum (12, 13).

There is great clinical need to identify and investigate premanifest HD gene carriers; i.e. those who have CAG expansions without motor symptoms and will gradually develop manifest HD. Since atrophy of both neuronal striatal and subcortical gray matter

Competing Interest: The authors declare no competing interest.
Received: July 19, 2023. **Accepted:** November 29, 2023

cells, as well as of non-neuronal skeletal muscle cells is an early sign of premanifest HD, our plan is to investigate the molecular signaling and, specifically, calcium signaling that regulates numerous cellular process affected by cell atrophy. In fact, calcium dysregulation is one of the striking features of HD. A study by Mattson (14) demonstrated that perturbation of intracellular calcium homeostasis is associated with neuronal death. Intracellular calcium imaging shows that mutant Huntingtin results in excessive basal calcium release (calcium leak via ryanodine receptor [RyR]) leading to depletion of internal calcium stores. Calcium leak has been observed in both striatal and cortical neurons in the R6/2 HD mice model (15).

We use a computer model to discern the effect of cell atrophy on the course of HD and how it might affect calcium dynamics in the cell. Such a study can guide our understanding of calcium-dependent molecular mechanisms affected in HD and inform our knowledge regarding the effectiveness of future therapy/drug development. Our goal is to understand how cell shrinkage affects some of the key cell signaling molecules/mechanisms in the course of HD and to better guide us on the effectiveness of possible drugs. Specifically, we simulated the effects of cell volume shrinkage on calcium handling and dynamics. A 3D computational model of calcium handling dynamics in a short segment of a neuronal axon was constructed using a stochastic, particle-based simulator, MCell4/CellBlender, to simulate molecular interactions.

After an action potential (AP), an influx of calcium through voltage-dependent calcium channels (VDCCs) into an axon triggers the activation of RyRs and subsequent calcium-induced calcium release (CICR) from the endoplasmic reticulum (ER).

Our realistic model of a reconstructed segment of an axon included the ER and the subcellular arrangement of molecules involved in calcium homeostasis and CICR after an AP, the critical stimulus that triggers a cascade of dynamic events involving calcium.

We found that the extent of accumulation of the released calcium in the cytosol is strongly dependent on the cytosolic volume. Our finding indicates that the restricted cell volume will result in a "positive feedback" mechanism in which calcium influx through the open VDCCs results in a local increase in $[Ca^{2+}]_{cyt}$. If this local transient is high enough it will activate the nearby RyRs, causing the release of Ca^{2+} from the ER that further elevates the local $[Ca^{2+}]_{cyt}$, which in turn incites even more RyRs via positive feedback and depletes ER calcium. The axon will remain in this feedback loop until the local $[Ca^{2+}]_{cyt}$ decreases below the activation threshold of RyRs. This prolonged increase in the $[Ca^{2+}]_{cyt}$ and accumulation in other organelles including mitochondria is highly toxic to the cell and can result in cell death (16).

Methods

Overview of MCell

The MCell4 computer program that we used to simulate the calcium dynamics in axons is a powerful modeling tool for realistic stochastic simulation of cellular signaling in subcellular microenvironments in and around cells (17). MCell was originally developed for use at synapses to study the behavior of molecular interactions in small compartments containing so few molecules that macroscopic continuum assumptions (especially the "well-mixed" assumption) do not apply and stochastic behavior dominates (18, 19). MCell4 uses highly optimized Monte Carlo algorithms and network-free particle-based evaluation of reaction rules, to track the stochastic behavior of individual molecules in space and time as they diffuse and interact within the cytosol and on membrane surfaces. In this program, molecules are represented as discrete particles with binding and modification sites that are acted upon by specified reaction rules expressed using the BioNetGen language (BNGL) (20). During a simulation, the rules are triggered stochastically according to the reaction rates when collisions between two particles are detected in the geometric space. The movements of molecules in 2D and 3D are simulated as a pseudo-random walk in accordance with the diffusion constants specified. Stochastic biochemical reaction networks are specified in BNGL with their chemical kinetic rate constants. The creation of the model was aided by using CellBlender, an add-on for the powerful 3D computer graphics modeling tool, Blender, and provides a Graphical User Interface for designing and implementing MCell4 models.

CellBlender enables model building of cellular systems with increasing scope and complexity. Such models can enable new insights by illustrating how microscopic interactions and their spatial organization give rise to macroscopic behavior. Because models constructed in this way include rich mechanistic detail, predictions from simulations constitute testable hypotheses at the biochemical and molecular biological levels (21, 22). The model simulates the function of a cellular system from its structure and component parts, including molecules, reaction networks, subcellular organelles, and cellular membrane architecture. The MCell4/CellBlender platform for cell modeling and simulation was developed and designed expressly for this purpose (17, 19, 22, 23).

Calcium-induced calcium release

Calcium is an essential signaling ion in cells in which many physiological stimuli rely on intracellular free calcium level (24, 25). In neurons, the cytosolic calcium concentration is important for determining neuronal activities and is modified by CICR, defined as the release of calcium from the ER into the cytosol triggered by an increase of calcium in the cytosol (26). This process was first discovered in skeletal muscle.

Neurons are equipped with a sophisticated homeostatic mechanism to keep the resting steady-state cytosolic calcium concentration in a tightly regulated range of around 100 nM (27). Among many calcium influx pathways, VDCCs are the major source of calcium influx into the cytosol from the extracellular space that is modulated by axonal and synaptic activity. In CICR, a relatively small increase in cytosolic calcium induces the opening of RyRs, located in the ER, allowing calcium stored in the ER to enter the cytosol. Activation of RyR causes "hotspots" of cytosolic calcium that cause further opening of ER calcium channels and promote mitochondrial calcium uptake. This makes ER a critical organelle that has the ability to act as an amplifier for cytosolic calcium elevation and is capable of generating calcium transients in the absence of significant plasma membrane depolarization. Calcium transients due to CICR have been described in neurons experimentally (28). Calcium amplification by CICR, demonstrated in numerous types of neurons including both the central and peripheral nervous system, has a role in the propagation of calcium increases that control neuronal membrane excitability and synaptic plasticity as well as gene expression (29).

RyRs are the major channels responsible for CICR from the ER of neurons that play an important role in HD pathology. However, CICR can also originate from Inositol 1,4,5-trisphosphate (IP3) receptors (IP3Rs) in the ER. Activation of IP3Rs requires concurrent binding of calcium and IP3. IP3 is generated by activation of cell signaling pathways with G-protein-coupled receptors. We have not included these pathways in our current model.

Model configuration

Figure 1 shows the schematic diagram of our model. Calcium-ATPases are the key components of calcium extrusion machinery that are also pivotal for the preservation of neuronal calcium homeostasis incorporated in our model. The plasma membrane calcium ATPase (PMCA) and sarco/endoplasmic calcium ATPase (SERCA) were identified decades ago and have a high affinity for calcium ions, maintain cytosolic calcium concentration in the resting steady state at ~100 nM, and restore this balance following muscle activation in response to a neuronal stimulus. In the schematic diagram in Fig. 1, the PMCA pumps (green) are located in the plasma membrane and the SERCA pumps (blue) are in the ER membrane.

PMCA pumps need ATP to pump calcium from the intracellular compartment of the cell to the extracellular region outside the cell, against a steep concentration gradient. The laws of thermodynamics require that PMCA pumps must also leak calcium from outside to inside. We assumed the inward leak flux of calcium through PMCA from outside to inside is constant because $[Ca^{2+}]_{out}$ is constant. The rate at which the PMCA pump extrudes calcium is directly proportional to $[Ca^{2+}]_{cyt}$. At rest, the inward leak flux balances the outward flux through the PMCA pump, thus establishing steady-state homeostasis, at 100 nM $[Ca]_{cyt}$. The ER calcium level is maintained by the sarcoendoplasmic reticulum calcium ATPase (SERCA) pumps. If $[Ca^{2+}]_{cyt}$ is at steady state, it will have a constant value of 100 nM and the inward flux through the SERCA pump into the ER will be constant. At rest, the outward flux from the SERCA pump is equal to the inward flux, which occurs when $[Ca^{2+}]_{ER}$ is 400 μM. In Fig. 1, Calbindin (gray) acts as a calcium buffer. The buffering provided by calbindin protects them against potentially harmful increases in intracellular calcium. At resting $[Ca]_{cyt}$ of 100 nM, only a small fraction of the calbindin will be bound by calcium. Dihydropyridine receptors (DHPR) VDCCs (also known as L-type VDCCs) (red) mediate voltage-dependent transients of calcium influx into the cytosol in response to APs and synaptic activity. The L-type VDCCs are associated with RyRs and are localized outside of the active zone (30). Axonal neurons also contain N-, P-, and Q-type VDCCs which are localized to the active zone of the axonal bouton and are not associated with RyRs (31) but are not included in our model. Calcium transients entering via VDCCs activate RyRs (white) on the ER and trigger CICR from the ER into the cytosol. During calcium transients, calbindin binds to the calcium according to its reaction kinetics and buffering capacity. If calcium transients are too large, the buffering capacity of calbindin can saturate, allowing the $[Ca^{2+}]_{cyt}$ to continue increasing. Following a calcium transient, the collaborative effects of PMCA and SERCA re-establish calcium homeostasis in the cytosol and ER compartments.

Model geometry

We constructed an axonal bouton using 3DEM (22), shown in Fig. 2A and B. Here, we started with the cytosolic volume, as obtained directly from the 3DEM, which we defined to be the full cytosolic volume (Fig. 2A, top). We then used the "shrink wrap" tool in Blender to shrink the net cytosolic volume in our model by 50%, without changing the volume of the ER or mitochondrion, to represent the 50% cytosolic volume case, and then further shrank the cytosol down to 20% cytosolic volume. We then distributed the pumps, channels, and buffers according to their known localization, and initial concentrations/densities, as visualized in Fig. 2B, from sources in the literature (see Table S1). We assumed that the density of PMCA remains constant with shrinkage of the axon due to a homeostatic mechanism which operates to maintain the PMCA density.

Molecules and their biochemical interactions

Figure 3 and Table S1 summarize the reaction kinetic schemes as well as rate constants in the model.

AP stimulus

Figure 4 shows the waveform of the AP in the axon used in our model. Membrane depolarization due to the AP (Fig. 4A), caused VDCCs to open (Fig. 4B) allowing an influx of calcium to trigger the activation of RyRs and subsequent CICR from the ER (see Results).

Calcium point-release stimulus

For the point-release of calcium (see supplementary material), a chosen number of calcium ions were simultaneously released at time $t = 0$ from a point in space very close to the cluster of RyRs. The number of calcium ions released was varied to assay the stimulus sensitivity as discussed in supplementary material.

Assay of sensitivity to stimulus

The sensitivity of the triggered activation of the RyRs was determined under different shrinkage states of the cytosolic volume. We varied the number of RyRs clustered on the ER to determine the threshold number of RyRs needed for the calcium in the ER to empty by 50% in response to a single AP.

Results

During an AP, the extent of accumulation of released calcium in the cytosol is strongly dependent on the cytosolic volume as shown for three simulated volumes in Fig. 5. The initial rapid decay of the calcium in the full volume case is due to the high capacity of calbindin to buffer the calcium. It is important to note that the concentration of calbindin is the same in all three models and this means that the total amount of calbindin available to buffer calcium is reduced by the same factor as the cytosolic volume in the models of cell shrinkage. Consequently, the initial decay of calcium at 50% volume is not as rapid as the full volume case due to the reduced capacity of calbindin in this shrinkage condition. The plateau in the 20% volume case indicates that the calcium accumulation in the shrunken cytosol has saturated the calbindin buffer as can be seen in Fig. 5.

We used the same concentration of calbindin in all models and the only change was in the volume, which alone was responsible for the decreased calbindin buffering capacity in these simulations. In HD, a decreased expression of the calbindin gene has also been reported (32), which will further contribute to the failure of calcium buffering in the cell and ultimately to calcium-mediated cytotoxic events.

Another interesting phenomenon is the "toxic positive feedback mechanism". As the volume of the cytosol decreases, RyR is more strongly activated, which leads to the depletion of calcium from the ER. As shown in Fig. 6, in the case of full volume, calcium is partially depleted; however, at 50 and 20% cytosolic volume, there is an almost complete emptying of the ER. This is an interesting phenomenon since the RyRs in our model function normally and the only change is in the volume. As the volume decreases, RyRs are activated much more strongly and act as if they are "leaky" (Fig. 7) as reported in HD (15). With full volume, only two

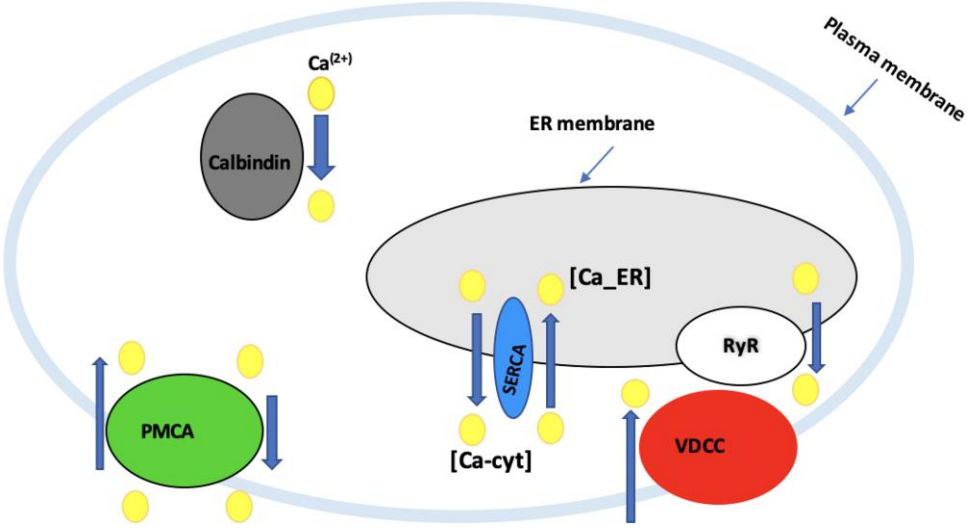

Fig. 1. Schematic diagram of subcellular compartmentalization and handling of calcium in cells. Cytosolic calcium (yellow) is maintained at homeostasis by PMCA pumps (green). ER calcium is maintained by SERCA pumps (blue). Calbindin (gray) buffers cytosolic calcium. VDCCs (red) allow voltage-dependent calcium influx into the cytosol which can activate RyRs (white) and trigger CICR from the ER into the cytosol. PMCA pumps and SERCA pumps then work to re-establish calcium homeostasis.

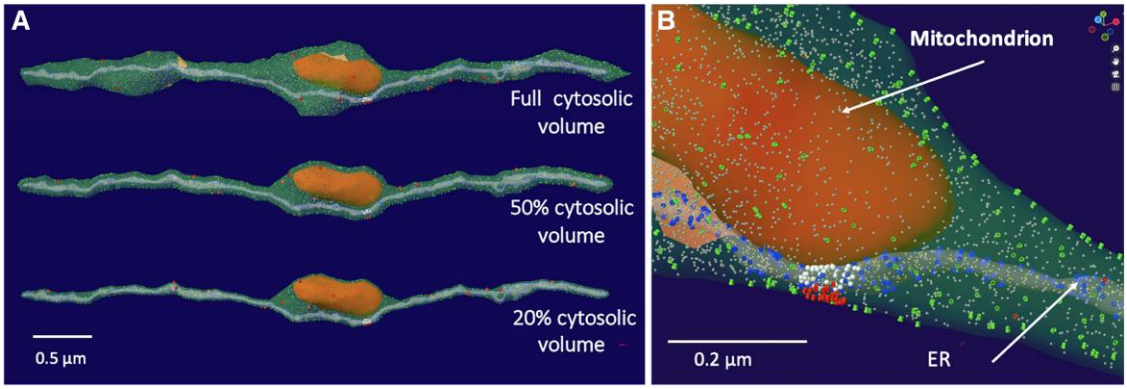

Fig. 2. Three models of cytosolic volume in a segment of the axon. Visualization of actual models at resting steady-state. A) Full cytosolic volume (top), 50% cytosolic volume (middle), and 20% cytosolic volume (bottom). B) Close-up of axon in the full cytosolic model in the region of the VDCC and RyR cluster. Calcium (yellow), PMCA (green), calbindin (gray), SERCA (blue), VDCC (red), and RyR (white).

RyRs open during the calcium transient initiated by the AP (Fig. 7, red curve), and close with a time constant of about 3 ms. Interestingly, at 50% volume (Fig. 7, green curve), only two RyRs open but they remain open for a prolonged period (decay time constant of about 125 ms) due to strong CICR feedback. At 20% volume, very strong CICR results in the opening of about seven channels with a prolonged plateau and a decay time constant of about 5 s. Note that when the RyRs are strongly activated, the rate of emptying of the ER in Fig. 6 is limited by the rate at which calcium can diffuse along the narrow ER and reach the cluster of RyRs. This limit has already been reached in the 50% volume case when only two channels are open (Fig. 7). Thus opening seven channels (in the 20% volume case, Fig. 7) cannot increase the rate of emptying by a significant amount (Fig. 6).

We designed an assay to quantify the sensitivity for triggering CICR in the three models of cytosolic volume. In our assay, we adjusted the number of RyR present in the patch of RyRs on the ER and measured the number of RyRs necessary to cause a 50% depletion of Ca from the ER when triggered by a single AP. Figure 8 shows that at full cytosolic volume, 50 RyRs are required to give 50% depletion, while 30 RyRs are required at 50% volume, and only five RyRs are required at 20% cytosolic volume.

We have found a drastic shift in the amplitude and time course of calcium-dependent dynamics from full volume (Figs. 5–7, 9, red curves) to 50% volume (Figs. 5–7, 9, green curves) due to volume shrinkage. This shift results in a "toxic" positive feedback mechanism producing prolonged activation of RyR and calcium release into the cytosol. The excessive calcium release from ER saturates the calcium buffer capacity of calbindin forcing further accumulation in the cytosol and cellular compartments including mitochondria. Excessive calcium accumulation in the cytosol can damage the mitochondria resulting in metabolic dysfunction in the cell consistent with the pathology of HD.

The intracellular calcium leak via RyR has been shown to have an important role in HD pathology. The mouse model of HD (Q175) also shows a leak via the ER resulting in cognitive dysfunctions and decreased parasympathetic tone associated with cardiac arrhythmias as well as reduced diaphragmatic contractile functioning resulting in impaired respiratory function. So leaky RyR has been reported to have an important role in neuronal, cardiac,

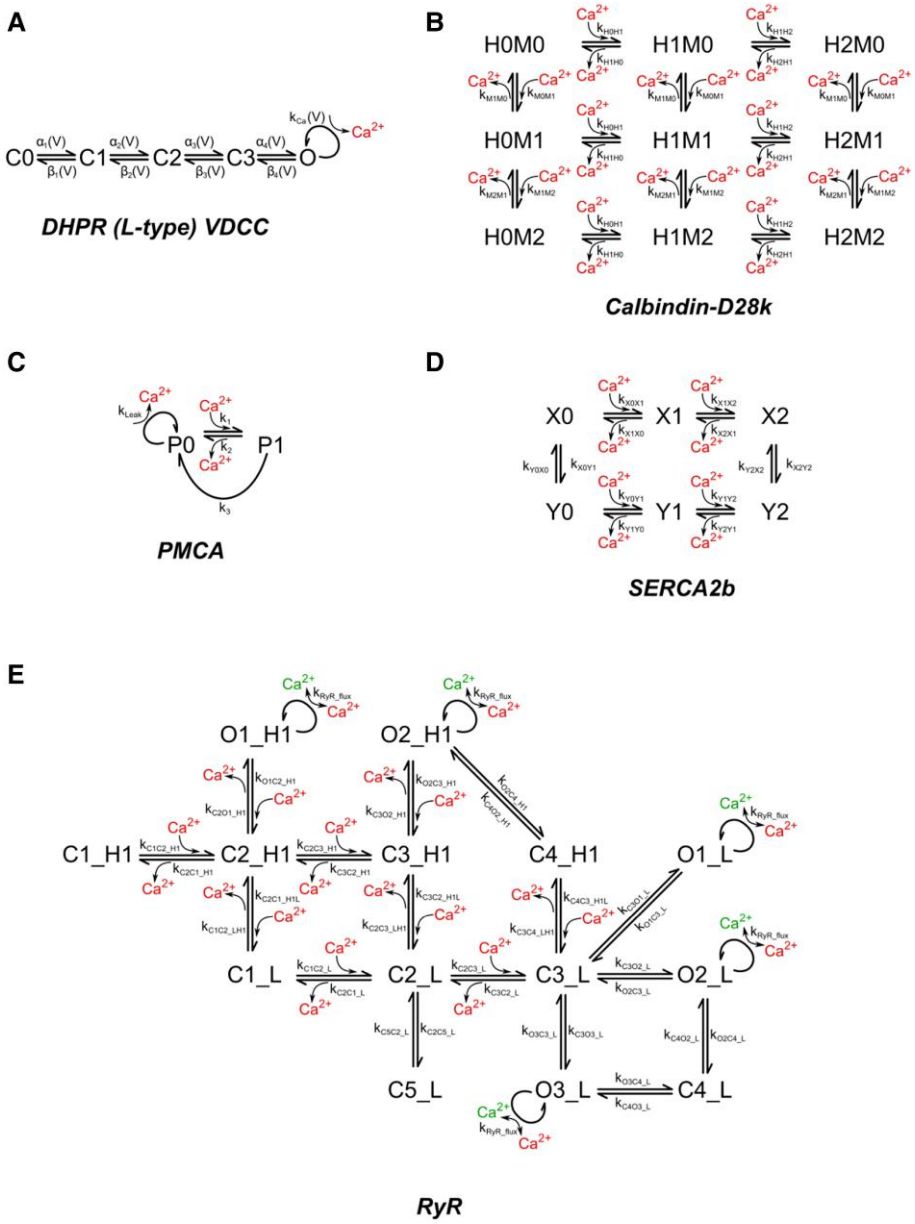

Fig. 3. Chemical kinetic reaction schemes. The reaction schemes with kinetic rate constants are shown for A) DHPR (L-type VDCCs); B) Calbindin-D28K; C) PMCA pumps; D) SERCA2b pumps; and E) RyRs. The values of the specified rate constants with references are given in Table S1.

and diaphragmatic pathophysiology in HD and RyR has been noted as a potential new therapeutic target. Rycal, a small-molecule drug (S107) that fixes leaky RyR might be a potential treatment for these dysfunctions (33). But note that our model suggests that functionally normal RyRs act as leaky RyRs when driven too hard by calcium transients as the limit of calbindin buffering capacity is reached. Thus, leaky RyRs might only be an indirect cause of dysfunction of calcium handling in HD. The upregulation of calbindin is another potential drug target.

Discussion

Fluctuation of calcium concentration acts as a signal for multiple processes in cells in general and especially in neurons. Calcium is an essential signaling ion that plays a crucial role in HD pathology. Our findings are consistent with many previous studies of HD and neurodegenerative diseases. Earlier studies also emphasize the importance of calcium dysregulation via L-VDCCs and RyRs and its role in memory deficits. It is shown that prolonged neuroinflammation results in elevation of proinflammatory cytokines and reactive oxygen species. This can lead to neuronal calcium homeostasis via L-type VDCCs and RyRs. Such chronic neuroinflammation can result in deficits in spatial memory (34).

In addition, studies indicate that neurons containing neurofibrillary tangles have an increased cytosolic calcium concentration. A study from cell lines that are obtained from Alzheimer's disease and the normal group shows upregulation of calcium in the disease state resulting in intracellular calcium overload and abnormal neuronal metabolism resulting in neuronal apoptosis and memory decline (35, 36). Calcium leak via RyR has an important role in neuronal death in HD (15) and is correlated with cognitive dysfunction and decreased parasympathetic tone leading to cardiac arrhythmias as well as reduced diaphragmatic contractile function that results in respiratory dysfunction (33). In R6/2

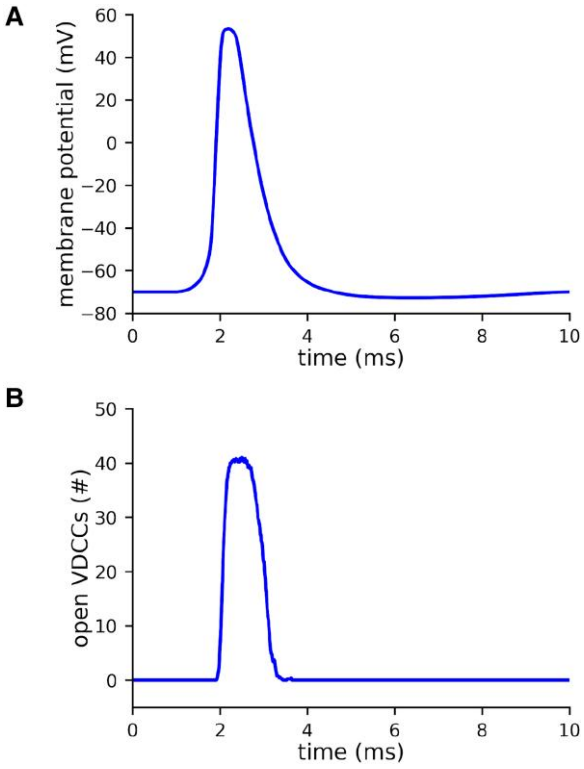

Fig. 4. AP and activation of VDCCs in the axon. (A) The AP waveform activates VDCCs (B) allowing an influx of calcium into the cytosol. Note that at the peak of the AP, all 41 of the VDCCs are open. The net Ca^{2+} ion flux through 41 VDCCs is ~15,000 ions during the ~1.5 ms duration of open VDCCs due to the AP.

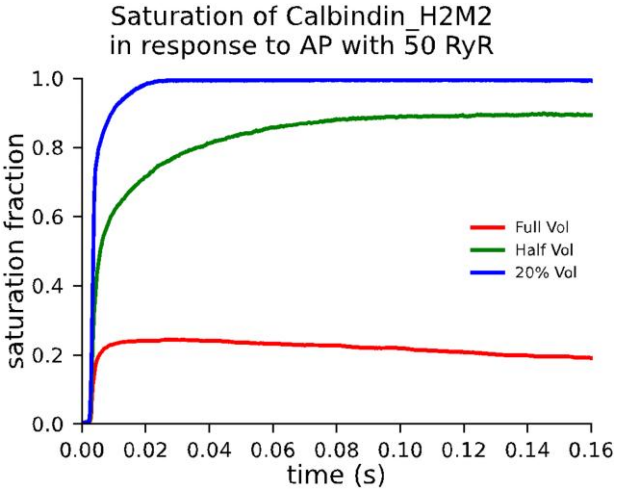

Fig. 5. Impact of cell shrinkage on the time course of saturation of calcium binding to calbindin. At full cytosolic volume (red), the calcium-binding capacity of calbindin is far from complete saturation. At 50% volume (green), saturation approaches 90% by 80 ms after the AP triggers CICR. At 20% volume (blue), the calbindin is completely saturated within 20 ms after the AP triggers CICR.

striatal and cortical neurons, elevated calcium levels and reduced ER calcium stored have been reported. RyR inhibition has been shown to be neuroprotective in vivo and improves motor behavior in YAC128 mice (37). In addition, in aging and in neurodegenerative diseases, significant decreases in the neuronal calcium-binding protein (28-kDa calbindin-D) gene expression

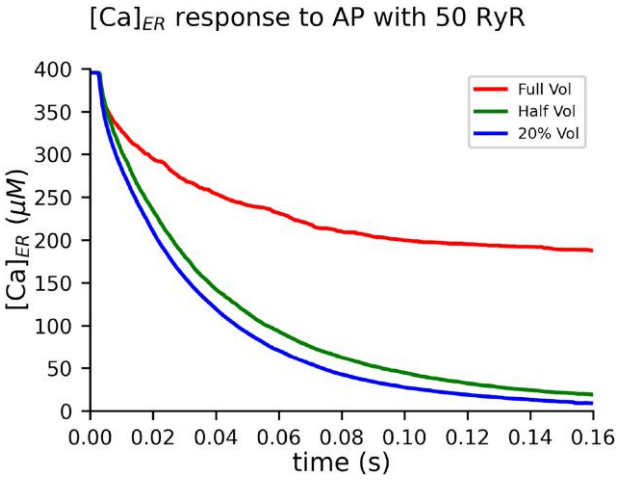

Fig. 6. Dependence of time course of calcium depletion from ER on cell shrinkage. At full cytosolic volume (red), the $[Ca^{2+}]_{ER}$ is only partially depleted by CICR triggered by AP with 50 RyR. But when the cytosol is shrunk to 50% volume (green) and 20% volume (blue), the stronger CICR in these conditions results in complete depletion of $[Ca^{2+}]_{ER}$.

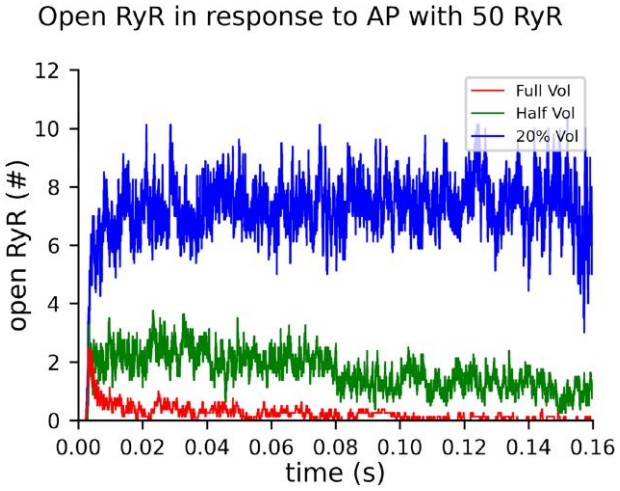

Fig. 7. Dependence of time course of open RyR on cell shrinkage. During CICR, an AP activates and opens DHPRs (see Fig. 3). If the calcium influx through the open DHPRs results in a high enough local $[Ca^{2+}]_{cyt}$, then nearby RyRs can also be activated and opened causing the release of Ca^{2+} from the ER which further elevates the local $[Ca^{2+}]_{cyt}$ and a further RyR activation through a positive feedback mechanism. At full cytosolic volume (red), CICR results in the activation of just two RyRs which close with a time constant of about 10 ms. At 50% cytosolic volume (green), CICR also results in the activation of about two RyRs, but the positive feedback is stronger due to the restricted cytosolic volume, resulting in greatly prolonged activation of the RyRs. At 20% cytosolic volume (blue), the restricted cytosolic volume results in the much greater initial activation of RyR by CICR and even greater prolongation of RyR opening. All curves represent the average of 8 simulations.

have been reported (32). Samples obtained from human brain tissue comparing a variety of neurodegenerative diseases with age and sex-matched control show a significant decrease (60–88%) in calbindin protein and mRNA in the substantia nigra in Parkinson's disease, in corpus striatum in HD, in the nucleus basalis in Alzheimer's disease and in the hippocampus and the nucleus dorsalis in Parkinson's, HD and Alzheimer's disease (32).

Important steps have been made using neuroimaging over the last four decades that have furthered our understanding of the

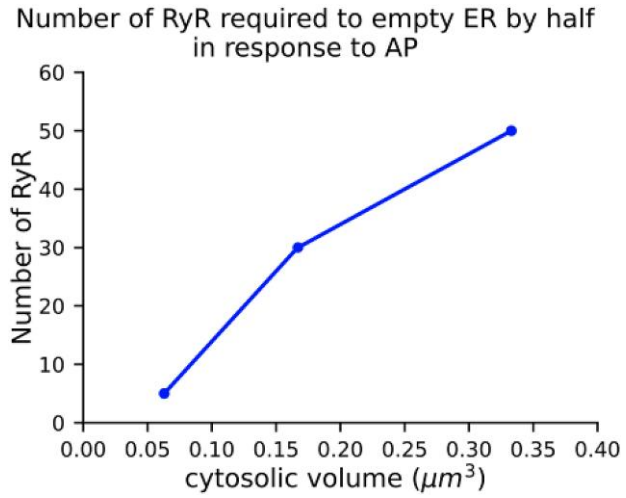

Fig. 8. Impact of shrinkage of cytosolic volume on the sensitivity of RyR activation. As the cytosolic volume decreases, RyR receptors are more strongly activated, and consequently fewer RyRs are required to empty calcium from the ER by 50%.

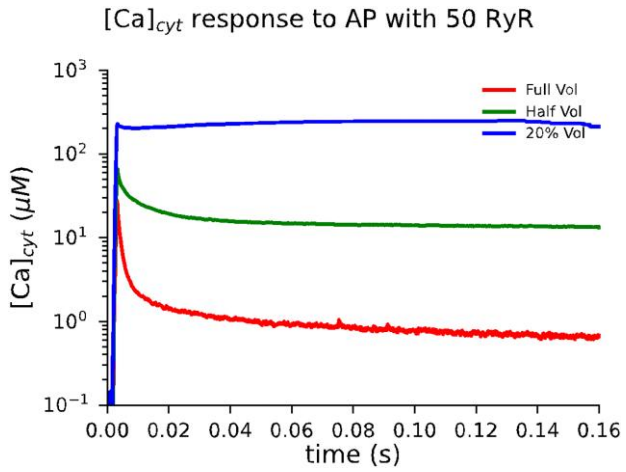

Fig. 9. Dependence of time course of calcium accumulation in the cytosol on cell shrinkage. After an AP, an influx of calcium through VDCCs triggers the activation of RyRs and subsequent CICR from the ER. The extent of accumulation of the released calcium in the cytosol is strongly dependent on the cytosolic volume. The three curves correspond to three volumes: full volume (red), half volume (green), and 20% volume (blue). The initial rapid decay of the calcium in the full volume case is due to the high calcium buffering capacity of the calbindin. The initial decay of calcium at 50% volume is not as rapid as the full volume case due to the reduced capacity of calbindin in the reduced volume. The plateau in the 20% volume case indicates that the calcium accumulation in the shrunken cytosol has saturated the calbindin buffer (see Fig. 5).

neural basis of HD. In particular, the demonstration of basal ganglia and cortical atrophy by structural brain imaging studies has provided strong in vivo evidence of cerebral structural changes in patients with HD (38). Our model indicates that the cell shrinkage alone can lead to RyR leaking and account for the decreased ER calcium storage, as well as saturation of calbindin in the cell and the inability of calbindin to buffer calcium effectively which further increases free calcium in the cell. In addition, we would expect that an increase in RyR expression, additional prolonged neuroinflammation that affect RyR activation, as well as decrease in calcium buffer calbindin would further amplify the impact of cell shrinkage.

To our knowledge, this is the first demonstration of how cell atrophy can affect important cell signaling at the molecular level and during the progression of HD. Future biological experiments can explore this prediction further and help pave the way for possible drug development for HD and similar neurological disorders. This study was intended to focus on HD but can also be used as a platform for other neurodegenerative studies and aging as well. This is significant since cell atrophy and dysfunction of calcium handling have been observed in many neurodegenerative diseases. In future studies, we will explore the potential therapeutic effects of available drugs that act on calbindin concentrations and calcium metabolism.

Acknowledgments

The authors thank members of the Computational Neurobiology Laboratory, especially Don Spencer, Claudia Lainscsek, and Mohammad Samavat for insightful discussions. S.S. is a grateful recipient of an HDSA Berman-Topper Family HD Career Development Fellowship.

Supplementary Material

Supplementary material is available at *PNAS Nexus* online.

Funding

This research was also supported by National Institutes of Health (NIH) P41GM103712, NIH MH095980-07, NIH MH115556, NIH MH129066, National Science Foundation (NSF) DBI-2014862, NSF DBI-1707356, NSF IIS-2219979.

Author Contributions

All authors participated in scientific discussion of this manuscript and commented on the manuscript. S.S. designed the research, performed the research as well as data analysis and wrote the article, and discussed the results. T.M.B. analyzed the data, and further helped edit the manuscript, and discussed the results. J.C.B. edited the manuscript and discussed the results. T.J.S. designed and supervised the research, and further edited the manuscript, and discussed the results.

Data Availability

All data reported are included in the main manuscript and supplementary material.

References

1 Sameni S, Syed A, Marsh JL, Digman MA. 2016. The phasor-FLIM fingerprints reveal shifts from OXPHOS to enhanced glycolysis in Huntington disease. *Sci Rep*. 6:34755.
2 Maria D, Laurie G, Nicole D, Emmanuel B. 2010. Mitochondria in Huntington's disease. *Biochim Biophys Acta*. 1802(1):52–61.
3 Tabrizi SJ, *et al.* 2011. Biological and clinical changes in premanifest and early stage Huntington's disease in the TRACK-HD study: the 12-month longitudinal analysis. *Lancet Neurol*. 10(1): 31–42.
4 Van den Bogaard SJA, *et al.* 2011. Early atrophy of pallidum and accumbens nucleus in Huntington's disease. *J Neurol*. 258(3): 412–420.

5 Halliday GM, *et al.* 1998. Regional specificity of brain atrophy in Huntington's disease. *Exp Neurol*. 154:663–672.
6 Aylward EH, *et al.* 2011. Longitudinal change in regional brain volumes in prodromal Huntington disease. *J Neurol Neurosurg Psychiatry*. 82(4):405–410.
7 Aziz NA, *et al.* 2008. Weight loss in Huntington disease increases with higher CAG repeat number. *Neurology*. 71:1506–1513.
8 Mochel F, *et al.* 2007. Early energy deficit in Huntington disease: identification of a plasma biomarker traceable during disease progression. *PLoS One*. 2:e647.
9 Robbins AO, Ho AK, Barker RA. 2006. Weight changes in Huntington's disease. *Eur J Neurol*. 13:e7.
10 Almeida S, Sarmento-Ribeiro AB, Januário C, Rego AC, Oliveira CR. 2008. Evidence of apoptosis and mitochondrial abnormalities in peripheral blood cells of Huntington's disease patients. *Biochem Biophys Res Commun*. 374:599–603.
11 Ciammola A, *et al.* 2006. Increased apoptosis, Huntingtin inclusions and altered differentiation in muscle cell cultures from Huntington's disease subjects. *Cell Death Differ*. 13:2068–2078.
12 de la Monte SM, Vonsattel JP, Richardson EP Jr. 1988. Morphometric demonstration of atrophic changes in the cerebral cortex, white matter, and neostriatum in Huntington's disease. *J Neuropathol Exp Neurol*. 47(5):516–525.
13 Heinsen H, *et al.* 1994. Cortical and striatal neurone number in Huntington's disease. *Acta Neuropathol*. 88(4):320–333. https://doi.org/10.1007/BF00310376
14 Mattson MP. 2007. Calcium and neurodegeneration. *Aging Cell*. 6:337–350.
15 Mari S, Yoshitaka N, Wada K, Koike T. 2012. Calcium leak through ryanodine receptor is involved in neuronal death induced by mutant Huntingtin. *Biochem Biophys Res Commun*. 429(1–2):18–23.
16 Bonora M, *et al.* 2020. Physiopathology of the permeability transition pore: molecular mechanisms in human pathology. *Biomolecules*. 10:998.
17 Adam H, *et al.* 2024. MCell4 with BioNetGen: a Monte Carlo simulator of rule-based reaction-diffusion systems with Python interface. *PLoSCompBio*. bioRxiv. https://doi.org/10.1101/2022.05.17.492333
18 Bartol TM Jr, Land BR, Salpeter EE, Salpeter MM. 1991. Monte Carlo simulation of miniature endplate current generation in the vertebrate neuromuscular junction. *Biophys J*. 59(6):1290–1307. https://doi.org/10.1016/S0006-3495(91)82344-X
19 Stiles JR, Bartol TM. 2001. Monte Carlo methods for simulating realistic synaptic microphysiology using MCell. In: de Schutter E, editor. *Computational neuroscience: realistic modeling for experimentalists*. CRC Press. p. 87–127.
20 Harris LA, *et al.* 2016. BioNetGen 2.2: advances in rule-based modeling. *Bioinformatics*. 32(21):3366–3368. https://doi.org/10.1093/bioinformatics/btw469
21 Coggan JS, *et al.* 2005. Evidence for ectopic neurotransmission at a neuronal synapse. *Science*. 309(5733):446–451.
22 Bartol TM, *et al.* 2015. Computational reconstitution of spine calcium transients from individual proteins. *Front Synaptic Neurosci*. 7:17. https://doi.org/10.3389/fnsyn.2015.00017
23 Kerr RA, *et al.* 2008. Fast Monte Carlo simulation methods for biological reaction-diffusion systems in solution and on surfaces. *SIAM J Sci Comput*. 30(6):3126. https://doi.org/10.1137/070692017
24 Berridge MJ. Capacitative calcium entry. *Biochem J*. 312(Pt 1)(Pt 1):1–11. https://doi.org/10.1042/bj3120001
25 Clapham DE. 1995. Calcium signaling. *Cell*. 80(2):259–268. https://doi.org/10.1016/0092-8674(95)90408-5
26 Endo M. 2009. Calcium-induced calcium release in skeletal muscle. *Physiol Rev*. 89(4):1153–1176. https://doi.org/10.1152/physrev.00040.2008
27 Grienberger C, Konnerth A. 2012. Imaging calcium in neurons. *Neuron*. 73(5):862–885. https://doi.org/10.1016/j.neuron.2012.02.011
28 Collin T, Franconville R, Ehrlich BE, Llano I. 2009. Activation of metabotropic glutamate receptors induces periodic burst firing and concomitant cytosolic Ca2+ oscillations in cerebellar interneurons. *J Neurosci*. 29:9281–9291.
29 Verkhratsky A. 2005. Physiology and pathophysiology of the calcium store in the endoplasmic reticulum of neurons. *Physiol Rev*. 85(1):201–279. https://doi.org/10.1152/physrev.00004.2004
30 Ouardouz M, *et al.* 2003. Depolarization-induced Ca^{2+} release in ischemic spinal cord white matter involves L-type Ca^{2+} channel activation of ryanodine receptors. *Neuron*. 40(1):53–63. https://doi.org/10.1016/j.neuron.2003.08.016
31 Eguchi K, Montanaro J, Le Monnier E, Shigemoto R. 2022. The number and distinct clustering patterns of voltage-gated calcium channels in nerve terminals. *Front Neuroanat*. 16:846615. https://doi.org/10.3389/fnana.2022.846615
32 Iacopino AM, Christakos S. 1990. Specific reduction of calcium-binding protein (28-kilodalton calbindin-D) gene expression in aging and neurodegenerative diseases. *Proc Natl Acad Sci U S A*. 87:4078–4082.
33 Dridi H, *et al.* 2020. Role of defective calcium regulation in cardiorespiratory dysfunction in Huntington's disease. *JCI Insight*. 5:e140614.
34 Hopp SC, *et al.* 2015. Calcium dysregulation via L-type voltage-dependent calcium channels and ryanodine receptors underlies memory deficits and synaptic dysfunction during chronic neuroinflammation. *J Neuroinflammation*. 12:56.
35 Perl DP, Gajdusek DC, Garruto RM, Yanagihara RT, Gibbs CJ. 1982. Intraneuronal aluminum accumulation in amyotrophic lateral sclerosis and Parkinsonism-dementia of Guam. *Science*. 217:1053–1055.
36 Selkoe DJ, Abraham C, Ihara Y. 1982. Brain transglutaminase: in vitro crosslinking of human neurofilament proteins into insoluble polymers. *Proc Natl Acad Sci USA*. 79:6070–6074.
37 Chen X, *et al.* 2011. Dantrolene is neuroprotective in Huntington's disease transgenic mouse model. *Mol Neurodegener*. 6:81.
38 Montoya A, Price BH, Menear M, Lepage M. 2006. Brain imaging and cognitive dysfunctions in Huntington's disease. *J Psychiatry Neurosci*. 31:21–29.